Paper pa02-065
Submitted to the 28th International Conference on High Energy Physics
ICHEP'96, Warsaw, Poland, July 1996

Electroproduction of ρ Mesons with Proton Diffractive Dissociation at $Q^2 > 7\,\mathrm{GeV}^2$ at HERA

H1 Collaboration

Abstract

The production of ρ^0 mesons with proton diffractive dissociation at $Q^2 > 7\mathrm{GeV}^2$ is studied in e^+p collisions at HERA with the H1 detector, for an integrated luminosity of 2.8 pb^{-1}. Events containing only a positron identified in the backward electromagnetic calorimeter, two charged particles in the tracking detector with reconstructed mass in the ρ^0 resonance mass region and fragments of the excited proton system registered in the forward detectors are used in the analysis. The ratio between proton dissociative and elastic cross sections is measured and found to be approximately constant in four (Q^2, W) intervals. The differential cross sections for proton dissociative ρ^0 meson production are derived as a function of P_t^2 (approximately equal to $|t|$), Q^2 and ρ meson polarisation. The results are discussed in the light of a factorisation hypothesis of the diffractive vertices.

1 Introduction

Vector meson production in lepton proton collisions is a powerful probe of the nature of diffraction. This process can be treated as the quasielastic scattering of the virtual photon on the proton. Following this approach the $\gamma^* p \to Vp$ process is usually called *elastic* (fig.1a) while the $\gamma^* p \to VY$ process is called *proton dissociative* (fig.1b), where V is a vector meson and Y is a low mass excited state, carrying the proton quantum numbers. Recently many experimental results were obtained for elastic ρ^0, ϕ and J/ψ meson production in electroproduction [1, 2, 3, 4] (virtual photon, $Q^2 \gtrsim 5\,\mathrm{GeV}^2$, where Q^2 is the negative square of the four momentum transfer from the initial to the final lepton) and in photoproduction [5, 6, 7, 8, 9] (almost real photon, $Q^2 \approx 0$). However little is known about proton dissociative vector meson production [6], in contrast with studies at high energy proton colliders where the proton dissociation has been widely investigated [10, 11, 12, 13].

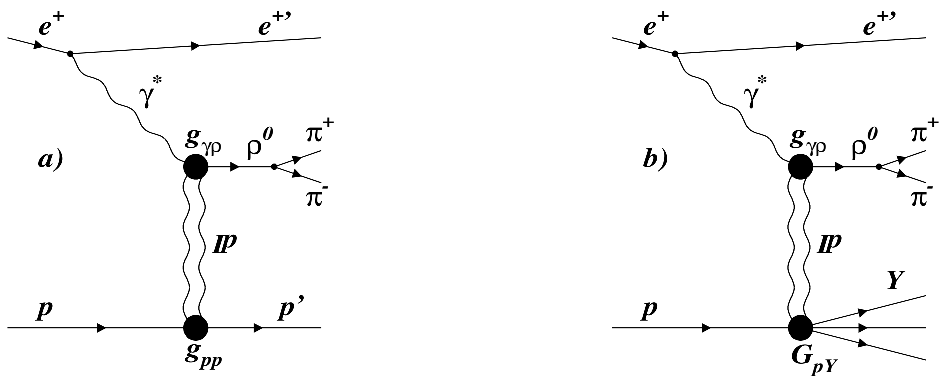

Figure 1: Diffractive ρ meson production: a) elastic scattering; b) proton dissociation.

Here we present briefly the phenomenological consequences following from different theoretical models describing diffractive vector meson production. Developed a long time ago, the Regge theory [14] explains several features of the different diffractive processes. In the framework of the Regge approach, the Vector Dominance Model (VDM) [15] is used to describe vector meson production. In this model the diffractive vector meson production is interpreted as being due to a fluctuation of the photon into a virtual vector meson, with subsequent scattering of this vector meson on the proton. Regge theory interprets diffraction as pomeron exchange and predicts a weak energy variation of the vector meson production cross section. The energy dependence was parametrised using the data from the proton colliders as $\sigma_{el} \sim W^{4\delta}$, where $\delta = 0.0808$ and W is the total hadron - proton energy [16]. A basic feature of diffractive processes is an exponential fall of the cross section as a function of t in the low $|t|$ region, where t is the squared four momentum transfer from the initial proton to the final proton or the excited system Y. In the Regge approach the slope of the diffractive peak is expected to increase with W as $b(W) = b(W_0) + 2\alpha' \ln(W^2/W_0^2)$, where α' is a slope of the effective pomeron Regge trajectory.

The hypothesis of factorization of the diffractive vertex [17, 18, 19] naturally appears in the framework of Regge theory. The factorization implies that each amplitude is proportional to the product of coupling constants $g(t)$ at each vertex. Scaling relations between diffractive dissociation and elastic scattering follow from this approach. The cross section ratio of proton diffractive dissociation to elastic scattering can be expressed as

$$\frac{\mathrm{d}^2\sigma_{pdis}/\mathrm{d}t\,\mathrm{d}M_Y^2}{\mathrm{d}\sigma_{el}/\mathrm{d}t} = \left(\frac{\mathrm{g}_{\gamma^*\rho}(t,Q^2)\ \mathrm{G}_{pY}(t,M_Y)}{\mathrm{g}_{\gamma^*\rho}(t,Q^2)\ \mathrm{g}_{pp}(t)}\right)^2 = f(t,M_Y) \tag{1}$$

where M_Y is the mass of the excited proton system and G_{pY} can be calculated using a triple-pomeron vertex approach. According to eq.(1) the cross section ratio depends only on t and M_Y.

In the framework of QCD inspired models, there have been attempts to describe the pomeron as a two gluon exchange [20]. Nonperturbative QCD models lead to the same "soft" energy dependence of the ρ meson production cross section [16] as in the Regge approach. The elastic differential γ^*p cross section is predicted to fall as Q^{-6} [21]. Assuming helicity conservation between the initial γ^* and the final vector meson, longitudinal polarisation is expected to dominate in electroproduction [21].

Recently, perturbative QCD calculations have been performed by several groups to describe elastic vector meson production [22, 23, 24, 25, 26, 27]. An important prediction of these models is a rapid increase of the electroproduction cross section with $W_{\gamma p}$, as a consequence of the rise of the gluon distribution in the proton. The Q^2 dependence of the γ^*p cross section is predicted, as in the non-perturbative approach, to fall as Q^{-6} but, taking into account the evolution of the parton distribution and quark Fermi motion, the effective Q^2 distribution is expected to be less steep [26]. The b-slope of the diffractive peak is assumed to be rather independent of the total energy W in some perturbative QCD calculations [26], but not all [24]. Violation of the factorization is expected to rise with the increase of the contribution of perturbative processes [24].

The high energy positron-proton experiments at HERA provide the possibility to extract from the data the contribution of proton dissociation, if the fragments which are emitted from the excited proton system and which are boosted to the forward direction are registered with high efficiency. These experimental conditions are fulfilled for the H1 detector, where forward subdetectors effectively detect charged particles up to a pseudorapidity of 7.5. Recently first results were presented by the H1 collaboration for proton dissociation in the photoproduction of J/ψ mesons [6]. This cross section was found to be as large as the elastic one and its energy dependence to be slightly steeper than for the elastic cross section. The exponential slope parameter for the transverse momentum P_t^2 distribution was measured to be $b = 1.6 \pm 0.3 \pm 0.1\,\mathrm{GeV}^{-2}$. This value is a factor of 2.5 smaller than for J/ψ elastic photoproduction.

The detailed study of proton dissociation was performed in proton collider experiments [10, 11, 12, 13]. The cross sections and b-slopes for the proton dissociative processes are approximately a factor of $2-3$ smaller than for the elastic ones. The differential cross section $\mathrm{d}\sigma/\mathrm{d}M_Y^2$ exhibits an approximate $1/M_Y^2$ dependence. For the large M_Y region the slope parameter b is independent of M_Y, but for lower masses it increases with decreasing M_Y. The factorization hypothesis was tested experimentally for fixed target πp, Kp and pp collisions at 140-175 GeV/c incident particle momentum and found to be confirmed

[28]. The approximate factorisation holds in the region of ISR collider energies [13], however the decrease of the proton dissociative to elastic cross section ratio for SPS and TEVATRON collider energies indicates to the deviation from the factorisation [11].

In this paper we report the first results on ρ meson production with proton dissociation for $Q^2 > 7\,\mathrm{GeV}^2$. After the description of the H1 detector components relevant for the analysis and of the data sample selection the invariant $\pi^+\pi^-$ mass spectrum and the P_t^2 distribution are obtained for the proton dissociative data sample. The ratio between the proton dissociative and elastic cross sections is presented for the kinematical region $7 < Q^2 < 36\,\mathrm{GeV}^2$ and $60 < W < 180\,\mathrm{GeV}$. The same ratios are obtained in the $\gamma^* p$ system for four kinematic regions distributed into two W and two Q^2 intervals. Then the differential cross sections for proton dissociative ρ meson production are presented as a function of Q^2 and polarisation. A comparison with theoretical expectations is discussed and finally the results are summarized.

2 The H1 Detector and Event Selection

The data were collected in 1994 using the H1 detector operating at the positron proton storage ring HERA. An integrated luminosity of 2.8 pb^{-1} is used for this analysis, obtained during the major part of 1994, when the HERA collider was operated with positrons bunches of 27.5 GeV interacting with proton bunches of 820 GeV. The H1 detector is described in detail in [29].

The signature for proton dissociative ρ meson electroproduction events is the scattered positron identified in the backward electromagnetic calorimeter (BEMC), two tracks of opposite charges detected in the tracking system and fragments of the excited proton system emitted in a narrow cone with respect to the initial proton direction and tagged by the forward detectors. All tracks have to originate from a vertex situated in the nominal e^+p interaction region.

In this analysis the positron was identified as an electromagnetic cluster with an energy larger than 12 GeV, reconstructed in the BEMC and associated with a hit in the backward proportional chamber (BPC) placed in front of it at 141 cm from the nominal interaction vertex. The BEMC covers polar angles of $151° < \theta < 176°$. The BPC has an angular acceptance of $155.5° < \theta < 174.5°$. The BPC hit position is required to be further than 15 cm away from the beam axis in order to avoid the region close to the beam pipe. The distance in the BPC plane between the BPC hit and the corresponding projection of the centroid of the electromagnetic cluster in the BEMC is required to be smaller than 4 cm, while the mean distance being approximately 0.9 cm. The scattered positron polar angle θ is determined from the position of the BPC hit closest to the BEMC cluster and of the interaction vertex. The trigger used for the present analysis requires the presence of a total energy larger than 8 GeV deposited in the BEMC, outside a square of $32 \times 32\ \mathrm{cm}^2$ around the beam pipe.

The pions originating from the ρ meson decay are registered in the central tracking detector, consisting mainly of two coaxial cylindrical drift chambers. The charged particle momentum component transverse to the beam direction is measured in these chambers by the track curvature in the 1.15 T magnetic field generated by the superconducting solenoid which surrounds the inner detector, with the field lines directed along the beam axis. Two polygonal drift chambers with wires perpendicular to the beam direction, located respectively at the inner radius of the two coaxial chambers, are used for a precise measurement of the particle polar angle. Tracks which are reconstructed from at least 5 hits in the drift chambers, which have a transverse momentum larger than 0.1 GeV/c and which lie in the polar angle range $5^\circ < \theta < 170^\circ$ are accepted. For the present analysis, two tracks of opposite sign are required to be reconstructed in the tracking system. The vertex position is reconstructed using these tracks. To suppress beam-gas interactions, the vertex must be reconstructed within 30 cm of the nominal interaction point in z, which corresponds approximately to 3 times the width of the distribution of the vertex z coordinate, The z axis corresponds to the proton beam direction with zero position at the nominal interaction point. No other track linked to the interaction vertex is allowed in the tracking detector, except for the positron track.

The central tracking detector is surrounded by a finely segmented liquid argon calorimeter (LAr) that provides hadronic and electromagnetic energy measurements in the range $4^\circ < \theta < 153^\circ$. To separate the actual particle energy depositions from noise in the calorimeters only clusters with an energy larger than 0.5 GeV in the LAr calorimeter and 1.0 GeV in the BEMC are considered in the present analysis. In order to suppress background events with the additional particles depositing the energy in the calorimeters, no clusters are allowed in the LAr and the BEMC except for those associated with the scattered positron, with the π mesons from the ρ meson decay, or with particles with pseudorapidity $\eta_{min} > 2.5$ possibly originating from the decay of the proton dissociative system. Here η_{min} is the minimum pseudorapidity of the clusters in LAr, except for those associated with the pions from the ρ meson decay.

Proton dissociation events are tagged by at least one of the three following subdetectors, namely the forward part ($\eta_{min} > 2.5$) of the LAr calorimeter, the forward muon system (FM) and the proton remnant tagger (PRT). These subdetectors are sensitive to particles emitted directly from the excited proton system or scattered in the beam pipe wall or the other apparatus placed close to the beam pipe. The FM subdetector consists of 6 planes of drift chambers at $6 < z < 9$ m and covers an angular interval $3^\circ < \theta < 17^\circ$. The PRT is a set of scintillator planes at $z = 24$ m and covers an angular range of approximately $0.06^\circ < \theta < 0.25^\circ$. To suppress noise, at least two pairs of hits in the FM or at least one hit in PRT are required.

The luminosity system, monitoring the reaction $ep \to e\gamma p$, consists of two TlCl/TlBr crystal calorimeters. The electron tagger is located at z=-33 m and the photon detector at z=-103 m.

3 Kinematics and Cross Section Definition

Only two independent variables define the kinematics of $ep \to eX$ deep inelastic scattering at fixed center-of-mass energy $\sqrt{s}$. They are conventionally chosen among Q^2, W and the Bjorken scaling variables x and y. Two additional variables have to be introduced for the proton diffractive vector meson electroproduction process $ep \to e\rho M_Y$ in order to define the mass and emission angle of the excited proton system. In this analysis the set of variables Q^2, W, M_Y and t is chosen.

For the most accurate determination of the kinematical variables the "double angle" method [30] is applied in this analysis. With this method the precisely measured polar angles θ and γ of the scattered positron and of the ρ meson are used to compute the kinematical variables as follows:

$$Q^2 = 4E_e^2 \; \frac{\sin\gamma \; (1+\cos\theta)}{\sin\gamma + \sin\theta - \sin(\gamma+\theta)} \tag{2}$$

$$y = \frac{\sin\theta \; (1-\cos\gamma)}{\sin\gamma + \sin\theta - \sin(\gamma+\theta)} \tag{3}$$

$$x = Q^2/(ys) \tag{4}$$

$$W^2 = m_p^2 + Q^2 \; (1/x - 1) \tag{5}$$

$$E_e' = E_e(1-y) + Q^2/(4E_e), \tag{6}$$

where E_e and E_e' are the energies of the incident and scattered positrons.

Taking into account that for the present analysis the hadronic energy W is significantly larger than Q^2 and M_Y, the absolute value of t is equal to the system Y squared transverse momentum P_t^2 with high accuracy. This parameter is calculated from the transverse components of the scattered positron and of the ρ meson momenta :

$$P_t^2 = (P_x^{e'} + P_x^{\rho})^2 + (P_y^{e'} + P_y^{\rho})^2, \tag{7}$$

where the ρ meson momentum components are obtained from the measured decay products.

The cross section for ρ meson electroproduction can be converted into a $\gamma^* p$ cross section using the relation

$$\sigma(\gamma^* p \to \rho Y) = \; \sigma_T^{\gamma^* p} + \; \varepsilon \sigma_L^{\gamma^* p} = \frac{1}{\Gamma_T} \frac{\mathrm{d}^2\sigma_{tot}(ep \to e\rho Y)}{\mathrm{d}W \; \mathrm{d}Q^2}, \tag{8}$$

where $\sigma(\gamma^* p \to \rho M_Y)$ is the virtual photon-proton cross section, and $\sigma_T^{\gamma^* p}$ and $\sigma_L^{\gamma^* p}$ are its transverse and longitudinal parts,

$$\varepsilon = \frac{1-y}{1-y+y^2/2}, \tag{9}$$

ε being the polarisation parameter, close to 1 in the kinematical region studied here.

The flux of transverse virtual photons is calculated from the Q^2, y and W values:

$$\Gamma_T = \frac{\alpha_{em} \; (1+(1-y)^2)}{\pi \; W \; Q^2}. \tag{10}$$

Due to the limited statistics, the integrated flux is calculated for each bin using the Q^2 and W dependences extracted from the data and neglecting their correlations. The systematic uncertainties of the flux definition are estimated by varying the Q^2 and W distributions inside the statistical errors and are found to be $\sim 7\%$. An additional systematic uncertainty of the cross section arises from the luminosity measurement accuracy of $\sim 2\%$.

4 Data Selection and Mass Distribution

In addition to the selections described above, the following kinematical cuts are applied to avoid kinematical regions with low detector efficiency, large background contributions or large flux weights:

$$7 < Q^2 < 36 \text{ GeV}^2 \tag{11}$$

$$60 < W < 180 \text{ GeV} \tag{12}$$

$$\sum (E - P_z) > 53 \text{ GeV} \tag{13}$$

where the sum is over the energy and momentum of the pions from the ρ meson decay and the scattered positron, computed by applying the "double angle" method.

In order to suppress the contamination in the data sample of ϕ mesons faking ρ mesons, an "anti-ϕ" cut is applied. The K^+K^- mass is required to be larger than 1.05 GeV/c^2, where the charged particles reconstructed in the tracking system are assigned the K meson mass. This cut reduces also the ω meson background contribution. Finally "proton dissociative" and "elastic" data samples are selected respectively using the forward detectors.

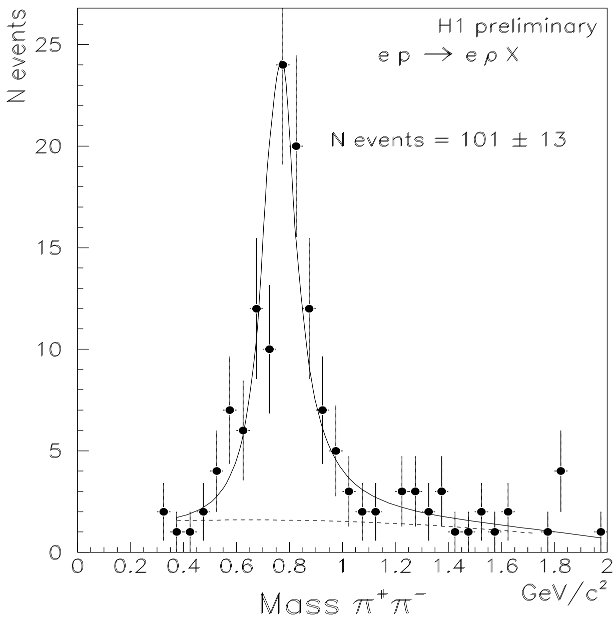

Figure 2: The invariant $\pi^+\pi^-$ mass spectrum. The solid curve represents the fit described in the text. The dashed curve shows the nonresonant background contribution.

The $\pi^+\pi^-$ invariant mass spectrum corresponding to the "proton dissociative" data sample is shown in Fig.2 for the kinematical region $P_t^2 < 0.8\,\text{GeV}^2$. A prominent peak is observed at the nominal ρ^0 meson mass position. The $\pi^+\pi^-$ mass spectrum is fitted with a relativistic Breit-Wigner function [31] to describe the ρ meson signal and a second order polynomial to describe the non-resonant background. The fit gives 101 $\pm$ 13 events corresponding to the ρ meson signal. The width Γ of the Breit-Wigner function is parameterised in the standard energy dependent form:

$$\Gamma = \Gamma_\rho \ (\frac{q^*}{q_0^*})^3 \ \frac{2}{1+(q^*/q_0^*)^2}. \tag{14}$$

Here q^* is the pion momentum in the $\pi^+\pi^-$ rest frame, and q_0^* is this momentum when $M_{\pi\pi} = M_\rho$. The mass and width Γ_ρ of the Breit-Wigner distribution are fixed to the nominal mass 769.9 GeV/c^2 and width 151.2 GeV/c^2 of the ρ meson [32]. The detector resolution smearing effects are estimated using a Monte Carlo simulation and found to be negligibly small.

5 Efficiency and Background Studies

Monte Carlo (MC) techniques are applied to determine efficiencies and to estimate backgrounds. Events are generated using models, of which the free parameters are adjusted using existing experimental results or theoretical predictions. The generated events are subjected to a detailed simulation of the H1 detector. The simulated events are processed through the same reconstruction and analysis chain as the data.

The proton dissociative electroproduction of ρ mesons is modelled by the DIFFVM MC generator [33]. The events are generated with an M_Y^2 squared mass distribution proportional to $1/M_Y^2$ for excited masses above 4 GeV/c^2. Below 4 GeV/c^2 the mass distribution is taken to follow to diffractive dissociation data obtained from deuterium measurements [18]. The system Y is fragmented at masses above 2 GeV/c^2 by treating it as a quark and diquark system and using the Lund string model [34]. Below 2 GeV/c^2 it is treated as a nucleon resonance and made to decay into nucleon and pions according to the known branching ratios. The systematic uncertainty arising from the statistical fluctuation of the MC efficiency determination is $\sim 2\%$. The accuracy of the MC determination of the forward detector efficiencies is estimated to be $\sim 7\%$ by comparing the relative probability of tagging by the different forward subdetectors in the MC and in the data. An additional contribution to the systematic uncertainty of $\sim 7\%$ is obtained by varying the power of the M_Y distribution from -1.5 to -2.5 and by comparing the standard Lund string fragmentation model with the extreme case of a KNO scaling and phase space decay fragmentation of the system Y.

Background processes to the proton dissociative ρ meson electoproduction were also studied using the MC technique. Three processes contribute mostly: elastic ρ meson production, standard deep inelastic scattering (DIS) and double dissociation of both the proton and the photon (DD). QED radiation effects have to be taken into account too.

Elastic ρ meson production was generated using also the DIFFVM generator. The probability to register the proton from elastic scattering in the PRT detector is found to be $1.0 \pm 0.2\%$. The probability for elastic events to fake proton dissociation because of noise in the forward detectors is estimated using statistics selected with random triggers, and found to be $1.0 \pm 0.2\%$ for the forward region of the LAr and $3.0 \pm 1.5\%$ for the FM system. The noise in the PRT is found to be $\sim 0.1\%$ and is neglected. Using the ratio of elastic to proton dissociative event numbers extracted from the data, the elastic background in the selected proton dissociative data sample is estimated to be $15 \pm 6\%$.

The standard deep inelastic scattering is simulated using the LEPTO 6.1 (MEPS) generator [35], which utilises $O(\alpha_s)$ matrix elements in QCD and parton showers. Applying the kinematical cuts described above, $6 \pm 2\%$ of the events in the proton dissociative data sample are predicted to be due to DIS. This number is checked from the data using the P_t^2 distribution. The background is estimated for the $0.6 < M_{\pi^+\pi^-} < 1.0\,\mathrm{GeV/c^2}$ mass region, where $\sim 81\%$ of the ρ meson signal is situated. The DIS contribution is steeply falling with increasing η_{min} and its P_t^2 distribution is expected to be significantly flatter than for the elastic and the proton dissociative processes. Thus the cuts $2.5 < \eta_{min} < 3.0$ and $P_t^2 > 2.0\,\mathrm{GeV}^2$ select the domain where the DIS background contribution is dominant. Extrapolating exponentially the P_t^2 distribution to the region with $P_t^2 < 0.8\,\mathrm{GeV}^2$, the DIS contribution in the proton dissociative data sample is found to be $6 \pm 4\%$, in a good agreement with the MC prediction.

The same technique is used to estimate the double dissociative background, applying the cuts $\eta_{min} > 3.0$ and $P_t^2 > 2.0\,\mathrm{GeV}^2$, selecting a region where the DD background dominates. The DD background in the region with $P_t^2 < 0.8\,\mathrm{GeV}^2$ is then estimated to be $6 \pm 5\%$. This leads to a total expected contribution from both the DIS and the DD backgrounds of $12 \pm 6\%$.

Only the resonant part of the DIS and DD backgrounds is important if we operate with the number of events obtained from the fit procedure. To extract the resonant part of these backgrounds, the invariant $\pi^+\pi^-$ mass spectrum for events in the $P_t^2 > 2.0\,\mathrm{GeV}^2$ region is fitted in the same way as for the original ρ signal. Assuming that the background slope is equal to $b_{bg} = 0.2 \pm 0.1\,\mathrm{GeV}^{-2}$ the resonant part of the DIS and DD backgrounds in the region $P_t^2 < 0.8\,\mathrm{GeV}^2$ is found to be $3 \pm 3\%$.

The background contribution from proton dissociative electroproduction of ϕ and ω mesons was checked using the DIFFVM MC and is found to be smaller than 1% after applying the "anti-ϕ" cut. The effects of QED photon radiation are simulated by the HERACLES 4.4 generator [36] and the corresponding correction factor is estimated to be 0.96 ± 0.03.

6 Slope of the P_t^2 Distribution

The efficiency corrected P_t^2 distribution is shown on Fig.3a for the selected events with a $\pi^+\pi^-$ invariant mass in the interval $0.6 < M_{\pi^+\pi^-} < 1.0\,\mathrm{GeV/c^2}$. The exponential slope parameter b_{pdis} is extracted from the fit of the P_t^2 spectrum assuming an $\exp(-b_{pdis}P_t^2)$ dependence of the proton dissociation cross section with the free b_{pdis} parameter, and exponential background distributions for the elastic scatering, DD and DIS with fixed shapes and the relative contributions estimated above. The background from elastic scattering is parameterised as exponentially falling with $b_{el} = 7.0 \pm 0.8 \pm 0.6\,\mathrm{GeV}^{-2}$ [2] and a relative contribution of $15 \pm 6\%$. The backgrounds from DD and DIS are parametrised with an exponential slope $b_{bg} = 0.2 \pm 0.1\,\mathrm{GeV}^{-2}$ and a relative contribution of $12 \pm 6\%$. The remaining 73% of the events are assumed to be due to ρ production with proton dissociation.

A fit in the region $P_t^2 < 1.2\,\mathrm{GeV}^2$ yields for the proton dissociative slope $b_{pdis} = 2.0 \pm 0.5 \pm 0.5\,\mathrm{GeV}^{-2}$. The first error is statistical and the second systematic. The systematic uncertainty originates mostly from the uncertainty of the background subtraction and the fit procedure. The systematic uncertainty arising from the background subtractions is estimated by varying the background contributions and slopes inside errors. The uncertainty of the fit procedure is estimated by varying the bin size, the bin position and the fitted P_t^2 region. The obtained slope for proton dissociation is about a factor three smaller than the elastic one.

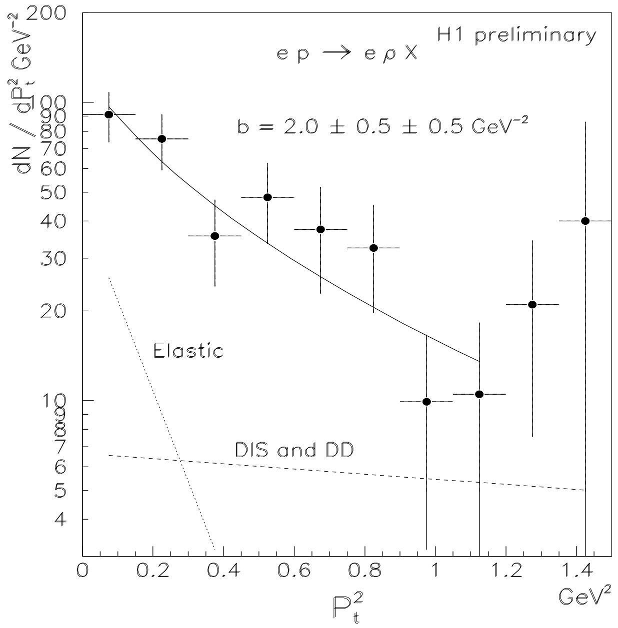

Figure 3: The efficiency corrected P_t^2 distribution for the proton dissociative data sample. The solid line represents the fit to the total distribution, with the elastic (dotted line), DD and DIS (dashed line) backgrounds fixed.

It has to be noted that, if the excited system Y has a small M_Y mass, the fragments of this system are emitted with very small angles with respect to the proton beam direction, and such events can not be efficiently tagged by the forward detectors. In this analysis the b-slope presented above thus corresponds approximately to the accessable kinematic domain $M_Y \gtrsim 1.6\,\mathrm{GeV/c^2}$. This has to be taken into account because in proton-proton collider experiments the exponential slope of the diffractive peak was observed to be steeper in the low M_Y mass region.

7 Ratio of Proton Dissociative to Elastic Cross Sections

The ratio of the proton dissociative to the elastic cross sections is calculated in the kinematical region $7 < Q^2 < 36\,\mathrm{GeV}^2$ and $60 < W < 180\,\mathrm{GeV}$. The numbers of events in the ρ meson signals with $P_t^2 < 0.8\,\mathrm{GeV}^2$ are obtained from the fit procedure described above. The numbers of events, the efficiencies and the correction factors are given in Table 1 for both the proton dissociative and the elastic scattering data samples.

	Proton dissociation	Elastic scattering	Ratio
Number of events	101 $\pm$ 13	291 $\pm$ 23	0.35 $\pm$ 0.05
Trigger efficiencies	0.99 $\pm$ 0.02	0.99 $\pm$ 0.02	1.00
Selection efficiencies	0.41 $\pm$ 0.01	0.57 $\pm$ 0.01	0.72 $\pm$ 0.01
Efficiencies of the $P_t^2 < 0.8\,\mathrm{GeV}^2$ cut	0.80 $\pm$ 0.10	1.00 $\pm$ 0.01	0.80 $\pm$ 0.10
Elastic bg. correction	0.85 $\pm$ 0.06		
Proton dissociation bg. correction		0.91 $\pm$ 0.08	
DD and DIS bg. corrections	0.88 $\pm$ 0.06	0.89 $\pm$ 0.06	
DD and DIS resonant bg. corrections	0.97 $\pm$ 0.03	0.98 $\pm$ 0.01	
Radiative corrections	0.96 $\pm$ 0.03	0.96 $\pm$ 0.03	1.00
Forward detectors off	1.10 $\pm$ 0.01	0.97 $\pm$ 0.01	
Fit procedure	1.00 $\pm$ 0.03	1.00 $\pm$ 0.03	1.00 $\pm$ 0.04

Table 1: Numbers of events, efficiencies and correction factors for the proton diffraction and the elastic scattering data samples.

Recently the H1 collaboration has published the results of the ρ meson elastic electroproduction study [2]. In the present analysis, applied Q^2 and pion angle cuts are relaxed. This leads to an increase in statistics, but also to a larger uncertainty in the event selection efficiency for the extended kinematical region. However these uncertainties cancel in the ratio of the proton dissociation to the elastic scattering cross sections, and thus do not lead to an increase in the systematic errors. The background contribution estimates were discussed in section 5 and in [2]. During data taking, the FM and PRT forward detectors were switched off for some periods, and the corresponding corrections are shown in Table 1. Additional factors are introduced to correct for the P_t^2 cut, the experimental uncertainties of the b-slope definitions being taken into account.

For the chosen kinematical region, the ratio of the proton dissociative to the elastic cross sections is:

$$\frac{\sigma(ep \to e\rho Y)}{\sigma(ep \to e\rho p)} = 0.63 \pm 0.11 \pm 0.11. \tag{15}$$

The first error is statistical and the second error is systematic. The latter uncertainty is dominated by the background estimates, the fit procedure and the efficiency determinations.

The data are grouped in four (Q^2, W) bins to study any variation of this ratio. The results are presented in Table 2. Flux factors are applied to convert the ρ meson electroproduction into a $\gamma^* p$ cross section. Within errors, no W or Q^2 dependence of the ratio is observed.

	$8 < Q^2 < 36\,\mathrm{GeV}^2$
	$60 < W < 180$ GeV
$\frac{\sigma(\gamma^* p \to \rho Y)}{\sigma(\gamma^* p \to \rho p)}$	$0.65 \pm 0.12 \pm 0.12$

	$8 < Q^2 < 16\,\mathrm{GeV}^2$	
	$60 < W < 120$ GeV	$120 < W < 180$ GeV
$\frac{\sigma(\gamma^* p \to \rho Y)}{\sigma(\gamma^* p \to \rho p)}$	$0.64 \pm 0.16 \pm 0.12$	$0.65 \pm 0.23 \pm 0.12$
	$16 < Q^2 < 36\,\mathrm{GeV}^2$	
	$60 < W < 120$ GeV	$120 < W < 180$ GeV
$\frac{\sigma(\gamma^* p \to \rho Y)}{\sigma(\gamma^* p \to \rho p)}$	$0.78 \pm 0.35 \pm 0.15$	$0.62 \pm 0.38 \pm 0.12$

Table 2: Ratios of the proton dissociative to the elastic $\gamma^* p$ cross sections for four kinematical intervals.

8 Q^2 and Polarisation Dependences

For the Q^2 and polarisation measurements the proton dissociative data sample is further restricted to the range $P_t^2 < 0.8\,\mathrm{GeV}^2$ and $0.6 < M_{\pi^+\pi^-} < 1.0\,\mathrm{GeV/c}^2$. The efficiency corrected Q^2 dependence for the $\gamma^* p \to \rho X$ cross sections is shown in Fig.4a. This distribution is fitted by a Q^{-n} function and the value $n = 5.6 \pm 1.2 \pm 0.6$ is obtained from the fit. The corresponding contributions of elastic scattering, DD and DIS are subtracted in the fit, the DIS and DD backgrounds with a power parameter equal to $n = 3.0 \pm 0.5$ and the elastic scattering background with $n = 5.0 \pm 1.0 \pm 0.4$ [2]. The systematic error includes mostly the uncertainties from the background subtraction, the fit procedure and the flux definition. It is calculated in the same way as for the P_t^2 distribution. The Q^2 dependence is consistent with that for the elastic electroproduction within errors.

The acceptance corrected $\cos\theta^*$ angular distribution is shown in Fig.4b. The angle θ^* is the angle in the ρ meson rest frame between the direction of the π^+ and the direction of the ρ meson in the $\gamma^* p$ center of mass system. The angle distribution is expected to be different for the different helicity states : $\propto \cos^2\theta^*$ for longitudinally polarised ρ mesons and $\propto \sin^2\theta^*$ for transversely polarised ρ mesons. The probability r_{00}^{04} for the ρ meson to be longitudinally polarised is obtained from the fit after background subtractions. A flat distribution is assumed for DD and DIS and the parameter $r_{00}^{04} = 0.73 \pm 0.05 \pm 0.02$ (see [2]) is used for the elastic scattering background subtraction. The fit gives $r_{00}^{04} = 0.78 \pm 0.10 \pm 0.05$, again in a good agreement with the elastic scattering data value. The systematic uncertainties are evaluated in the same way as for the P_t^2 distribution and are mostly due to the uncertainties of the background subtraction and the fit procedure.

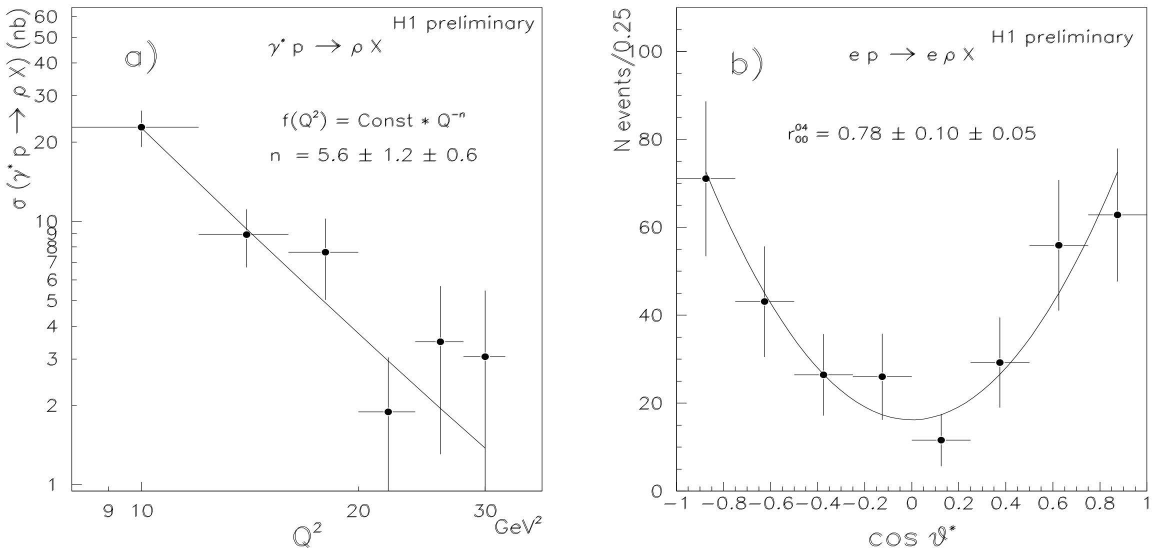

Figure 4: a) Q^2 distribution of the proton dissociative ρ meson electroproduction cross section after efficiency correction. The solid curve represents a fit with the Q^{-n} function, the backgrounds being taken into account in the fit procedure. b) Efficiency corrected polarisation distribution, the backgrounds being subtracted in the fit.

9 Test of the Factorisation Hypothesis

The results obtained for $\gamma^* p$ elastic scattering can be compared with other diffractive processes in the framework of the factorisation hypothesis using eq.(1). For example, in the case of proton-proton collisions the coupling constant $g_{\gamma^*\rho}$ is replaced by g_{pp}, which cancels in the ratio.

Assuming an exponential t dependence of the elastic and proton dissociative processes and an universal M_Y dependence of proton dissociation (both assumptions are in a good agreement with the experimental data for the low $|t|$ region) the cross section ratio after integration over M_Y is expected to be:

$$\frac{\sigma_{pdis} b_{pdis}}{\sigma_{el} b_{el}} \exp((b_{el} - b_{pdis})t) = f(W,t), \tag{16}$$

where σ_{el} and σ_{pdis} are the elastic and proton dissociative cross sections integrated over t. Energy dependence may appear due to the increase of the effective M_Y region with increasing energy.

This leads to:

$$\frac{\sigma_{pdis} b_{pdis}}{\sigma_{el} b_{el}} = f_1(W) \tag{17}$$

and

$$b_{el} - b_{pdis} = f_2(W). \tag{18}$$

If factorisation holds, the f_1 and f_2 values are expected to be the same for different diffractive processes for the same total center-of-mass energy. The f_1 and f_2 values for

γp interactions and pp interactions are compared in Tab.3, where respectively proton-proton and photon-proton center-of-mass energies are presented. The energy dependence is expected to be weak because the similar M_Y regions are effectively used in the measurements, and b-slopes depend on energy only logarithmically.

Experiment	ISR, pp	H1, $\gamma^* p \rightarrow \rho$	H1, $\gamma p \rightarrow J/\psi$
cms energy, GeV	53	60 - 180	30 - 150
b_{el}, GeV^{-2}	13.1 ± 0.3	7.0 ± 1.0	4.0 ± 0.3
b_{pdis}, GeV^{-2}	6.5 ± 1.0	2.0 ± 0.7	1.6 ± 0.3
$\sigma_{pdis}/\sigma_{el}$	0.48 ± 0.03	0.65 ± 0.17	1.0 ± 0.2
f_1	0.24 ± 0.04	0.19 ± 0.08	0.40 ± 0.11
f_2, GeV^{-2}	6.6 ± 1.0	5.0 ± 1.2	2.4 ± 0.4

Table 3: The comparison of the f_1 and f_2 values for γp and pp collisions.

The ρ meson electroproduction data in the interval $7 < Q^2 < 36\,\mathrm{GeV}^2$ are consistent within errors with proton-proton ISR collider results [13]. On the other hand, the f_1 and f_2 values obtained in J/ψ photoproduction study [6] deviate from the ρ meson electroproduction ones. These results might be interpreted as an indication that perturbative processes are contributing less for ρ meson electroproduction in the Q^2 region studied here than for J/ψ meson photoproduction. However in view of the large experimental uncertainties of the data, no firm conclusion can be obtained whether factorisation holds or not.

10 Summary

The electroproduction of ρ mesons with proton diffractive dissociation has been measured at HERA with the H1 detector. The following results are obtained:

• The ratio of the proton dissociative to the elastic cross sections for the kinematical region $7 < Q^2 < 35\,\mathrm{GeV}^2$ and $60 < W < 180\,\mathrm{GeV}$ is measured to be $\sigma(e^+p \rightarrow e^+\rho^0 Y)/\sigma(e^+p \rightarrow e^+\rho^0 p) = 0.63 \pm 0.11 \pm 0.11$. No significant variation of this ratio is found for two W and two Q^2 kinematic intervals.

• The exponential slope of the P_t^2 distribution for proton dissociative ρ meson electroproduction is found to be $b_{pdis} = 2.0 \pm 0.5 \pm 0.5$ GeV^{-2}. This value is about a factor 3 smaller than the b-slope for elastic scattering.

• The Q^2 distribution for the $\gamma^* p \rightarrow \rho Y$ process is fitted well by a Q^{-n} dependence, with the power parameter equal to $n = 5.6 \pm 1.2 \pm 0.6$. This value agrees with the value $n = 5.0 \pm 1.0 \pm 0.4$ for elastic scattering.

• The probability r_{00}^{04} for the ρ meson to be longitudinally polarised is measured to be $r_{00}^{04} = 0.78 \pm 0.10 \pm 0.05$, in good agreement with the value $r_{00}^{04} = 0.73 \pm 0.05 \pm 0.02$ for elastic scattering. It demonstrates that ρ mesons are mostly longitudinally polarised also in the proton dissociative process.

The similarity in the Q^2 and polarisation behaviours of the proton dissociative and elastic ρ meson electroproduction, and the comparison in framework the factorisation hypothesis with proton-proton collider results suggest a weak correlation between the processes originating from different diffractive vertices.

Acknowledgments

We are grateful to the HERA machine group whose outstanding efforts have made and continue to make this experiment possible. We thank the engineers and technicians for their work in constructing and now maintaining the H1 detector, our funding agencies for financial support, the DESY technical staff for continual assistance, and the DESY directorate for the hospitality which they extend to the non–DESY members of the collaboration. We thank further A.B. Kaidalov for useful discussion.

References

[1] M. Derrick et al., ZEUS Coll., *Phys. Lett.* **B356** (1995) 601;
M. Derrick et al., ZEUS Coll., preprint DESY-96-067 (1996).

[2] S. Aid et al., H1 Coll., *Nucl. Phys.* **B468** (1996) 3.

[3] M. Arneodo et al., NMC Coll., *Nucl. Phys.* **B429** (1994) 503.

[4] J.J. Aubert et al., EMC Coll., *Nucl. Phys.* **B213** (1983) 1;
J. Ashman et al., EMC Coll., *Zeit. Phys.* **C39** (1988) 169.

[5] S. Aid et al., H1 Coll., *Nucl. Phys.* **B463** (1996) 3.

[6] S. Aid et al., H1 Coll., preprint DESY-96-037 (1996).

[7] M. Derrick et al., ZEUS Coll., *Zeit. Phys.* **C69** (1995) 39;
M. Derrick et al., ZEUS Coll. *Phys. Lett.* **B350** (1995) 120;
M. Derrick et al., ZEUS Coll., preprint DESY-96-002 (1996).

[8] R.M. Egloff et al., *Phys. Rev. Lett.* **43** (1979) 657;
D. Aston et al., *Nucl. Phys.* **B209** (1982) 56.

[9] U. Camerini et al., *Phys. Rev. Lett.* **35** (1975) 483;
M. Binkley et al., *Phys. Rev. Lett.* **48** (1982) 73;
B.H. Denby et al., *Phys. Rev. Lett.* **52** (1984) 795;
R. Barate et al., *Zeit. Phys.* **C33** (1987) 505;
P.L. Frabetti et al., *Phys. Lett.* **B316** (1993) 197.

[10] F. Abe et al., CDF Coll., *Phys. Rev.* **D50** (1994) 5518;
F. Abe et al., CDF Coll., *Phys. Rev.* **D50** (1994) 5535.

[11] M. Bozzo et al., UA4 Coll., *Phys. Lett.* **B147** (1984) 392;
D. Bernard et al., UA4 Coll., *Phys. Lett.* **B186** (1987) 227.

[12] R.E. Ansorge et al., UA5 Coll., *Zeit. Phys.* **C33** (1986) 175.

[13] J.C.M. Armitage et al., CHLM Coll., *Nucl. Phys.* **B194** (1982) 365;
N. Amos et al., *Phys. Lett.* **B120** (1983) 460.

[14] D.P. Roy and R.G. Roberts, *Nucl. Phys.* **B77** (1974) 240;
R.D. Field and G.C. Fox, *Nucl. Phys.* **B80** (1974) 367.

[15] J.J. Sakurai, *Phys. Rev. Lett.* **22** (1969) 981;
J.J. Sakurai and D. Schildknecht, *Phys. Lett.* **B40** (1972) 121;
T.H. Bauer et al., *Rev. Mod. Phys.* **50** (1978) 261.

[16] A. Donnachie and P.V. Landshoff, *Phys. Lett.* **B185** (1987) 403;
A. Donnachie and P.V. Landshoff, *Phys. Lett.* **B296** (1992) 227;
A. Donnachie and P.V. Landshoff, *Phys. Lett.* **B348** (1995) 213.

[17] H. Holtmann at al.., *Zeit. Phys.* **C69** (1996) 297.

[18] K. Goulianos, *Phys. Rep.* **101** (1983) 169.

[19] A.B. Kaidalov, *Phys. Rep.* **50** (1979) 157.

[20] F.E. Low, *Phys. Rev.* **D12** (1975) 163;
S. Nussinov, *Phys. Rev. Lett.* **34** (1975) 1268.

[21] J.R. Cudell, *Nucl. Phys.* **B336** (1990) 1.

[22] M.G. Ryskin, *Zeit. Phys.* **C57** (1993) 89.

[23] S.J. Brodsky et al., *Phys. Rev.* **D50** (1994) 3134.

[24] N.N. Nikolaev, B.G. Zakharov and V.R. Zoller *Phys. Lett.* **B366** (1996) 337;
J. Nemchik et al., *Phys. Lett.* **B374** (1996) 199.

[25] L.P.A. Haakman, A. Kaidalov and J.H. Koch, *Phys. Lett.* **B365** (1996) 411.

[26] L. Frankfurt, W. Koepf and M. Strikman, preprint TAUP-2290-95, hep-ph/9509311 (1995).

[27] I.F. Ginzburg and D.Yu. Ivanov, preprint hep-ph/9604437 (1996).

[28] D.S. Ayres et al., *Phys. Rev. Lett.* **37** (1976) 1724.

[29] I. Abt et al., H1 Coll., *The H1 detector,* preprint DESY-93-103 (1993).

[30] S. Bentvelsen, J. Engelen and P. Kooijman, Proc. of the Workshop on Physics at HERA, ed. W. Buchmüller and G. Ingelman, Hamburg 1992, Vol. 1, p. 23;
K.C. Hoeger, ibid., p. 43.

[31] J.D. Jackson, *Nuovo Cim.* **34** (1964) 1644.

[32] L. Montanet et al., *Review of Particle Properties, Phys. Rev.* **D50** (1994) 1173.

[33] B. List, *DIFFVM program, Diploma Thesis*, Techn. Univ. Berlin, unpubl. (1993).

[34] T. Sjöstrand, Computer Physics Commun. **39** (1986) 347;
T. Sjöstrand, and M. Bengtsson, Computer Physics Commun. **43** (1987) 367.

[35] G. Ingelman, *LEPTO* 6.1 unpublished program manual (1993);
H. Bengtsson, G. Ingelman and T. Sjöstrand, *Nucl. Phys.* **B301** (1988) 554.

[36] H. Spiesberger, *HERACLES* 4.4, unpublished program manual (1993);
A. Kwiatkowski, H. Spiesberger and H.-J. Möhring, *An event generator for ep interactions at HERA including radiative processes,* in: Proc. of the Workshop on Physics at HERA, ed. W. Buchmüller and G. Ingelman, Hamburg 1992, Vol. 3, p. 1294.